Journal of Renewable Materials

Tech Science Press

DOI: 10.32604/jrm.2024.054977

ARTICLE

Greener, Safer Packaging: Carbon Nanotubes/Gelatin-Enhanced Recycled Paper for Fire Retardation with DFT Calculations

Hebat-Allah S. Tohamy*

Cellulose and Paper Department, National Research Centre, Dokki, Giza, P.O. Box 12622, Egypt

*Corresponding Author: Hebat-Allah S. Tohamy. Email: hebasarhan89@yahoo.com

Received: 13 June 2024 Accepted: 14 October 2024 Published: 20 December 2024

ABSTRACT

Fire retardant CNTs/WPP/Gel composite papers were fabricated by incorporating bio-based carbon nanotubes (CNTs) recycled from mature beech pinewood sawdust (MB) and cellulosic waste printed paper (WPP) into a gelatin solution (Gel) and allowing the mixture to dry at room temperature. The CNTs within the WPP matrix formed a network, enhancing the mechanical and thermal properties of the resulting CNTs paper sheet. In comparison to pure WPP/Gel, CNTs/WPP/Gel exhibited superior flexibility, mechanical toughness, and notable flame retardancy characteristics. This study provides a unique and practical method for producing flame-retardant CNTs/WPP/Gel sheets, suitable for diverse industrial applications, especially packaging, where used paper materials pose a significant fire risk. Bio-CNT-based fire-resistant packaging offers enhanced safety during transportation and storage. The sheets demonstrated increased strength and stiffness, with optimal mechanical properties achieved at a 20% CNTs loading. Additionally, thermal stability was improved, as confirmed by thermogravimetric analysis (TGA) and differential thermogravimetry (DTG). Flame retardancy tests revealed a rise in LOI (Limiting Oxygen Index) values with increasing CNTs content, indicating the CNTs' effectiveness in inhibiting combustion. The compatibility of recycled paper, CNTs, and Gel suggests potential applications in industrial fields, capitalizing on the biocompatible and biodegradable nature of cellulose. Density functional theory (DFT) calculations using the B3LYP with the 6-31G(d) basis set were employed to optimize the stability of these compounds and elucidate their chemical interactions.

KEYWORDS

Carbon nanotubes; packaging; cellulosic waste printed paper; flame retardancy; DFT calculations

Nomenclature

E	Micro strain
σ	Dislocation density
E_a	Activation energy
E_T	Total energy
E_g	HOMO-LUMO energy gap
μ	Dipole moment

1 Introduction

Paper, considered a biodegradable and cost-effective material, is widely used in various applications such as packaging, printing materials, gypsum board, and insulation board as interior finishing material [1–5]. Due to their high cellulose content, paper sheets are highly flammable, making them unsuitable for application in modern materials where fire resistance is essential [1,6,7]. Burning paper releases harmful greenhouse gases including CO_2, into the atmosphere [8,9]. To address the issue of paper's flammability, flame retardants (FRs) are often used. Organohalogen chemicals, containing bromine and chlorine, are particularly effective FRs as they act as radical scavengers in gases, potentially reducing the risk of fire. However, these chemicals can also pose significant toxicological and environmental concerns [10,11]. For these reasons, certain halogenated FRs have been banned from the market. Despite their effectiveness at relatively low concentrations, replacing them has proven challenging [12–16]. As a result, the industry seeks efficient, cost-effective, biodegradable and environmentally friendly flame retardant technologies.

The unique qualities of carbon nanotubes (CNTs), including their mechanical strength and fire retardation capabilities, make them promising candidates for use as nano-fillers [17–20]. Due to their exceptional properties, including high specific strength, high temperature resistance, and other outstanding characteristics, CNTs are widely used as FRs [2,21,22]. FRs enhance the value of paper's inherent qualities by reducing toxicity and smoke production. They primary work by lowering the breakdown temperature of cellulose, which reduces the production of levoglucosan, and by catalyzing dehydration and decomposition processes, which increases the formation of char [23]. Additionally, the high concentration of conventional FRs added today often reaching 40 wt% can lead to toxilogical effects. In contrast, CNTs demonstrate excellent flame-retardant properties even at low concentrations of 2 wt% [21]. CNTs are also a sustainable, economical, and recyclable material. Due to their distinctive hollow tubular form and nanoscale size, CNTs are used as a reinforcement material in composites by improving the stiffness and toughness of them [17,21]. Due to its biocompatibility, cellulose is a promising candidate for the development of CNTs–composite materials [17,22]. The use of sustainable composites offer several benefits; including biocompatibility and reduced energy consumption during producton [24]. Agricultural wastes are abundant, environmentally friendly materials that can be recycled into various products. Cellulose, the primary component of these wastes is a valuable resource for the production of composite materials [25,26]. Mature beech pinewood sawdust (MB), an agricultural waste product, can be utilized for the preparation of CNTs [17].

After disposal, paper can be reused, incinerated with or without energy recovery, or landfilled. However, burning paper and wood can pose environmental risks. By transforming WPP resources into valuable products, their harmful effects on the environment can be mitigated. Industrial utilization of waste materials reduces the costs of raw materials and the energy required to produce finished goods [27,28]. Flame retardancy is a desirable property of recycled papers that can be achieved through various methods. One such method involves dispersing CNTs into the WPP [22,29–31]. A significant challenge in developing CNTs-based flame retardants is the tendency of CNTs to aggregate within polymer matrices, leading to poor compatibility with the polymer material [22,32–35]. To address these challenges, biofriendly materials like gelatin (Gel) are used to disperse CNTs. G coats the CNTs, facilitating their dispersion in water without affecting their physical properties [22].

Currently, the preparation technique, mechanical properties, and thermal properties are the key areas of interest for research on the R1 (i.e., contains zero CNTs), R2 (contains 10 mg CNTs) and R3 (contains 20 mg CNTs). However, in order to guarantee inherent safety and expand its application in more domains, the flame performance of polymer composites is important. Previous studies didn't focus on the sustainability of the used polymers. Here, we prepare CNTs from agricultural waste in an easy, simple, and readily scalable process. The used cellulose was from the WPP. Studies are being done to change the composites made of

recycled papers as described above by examining the flame-retardant characteristics of conventional and nano flame-retardants. In this study, solution blending was used to create the CNTs/WPP/Gel composites. Thermal stability, DFT calculations and flame retardancy were investigated. Tensile tests assessed the material's mechanical properties.

2 Experimental

2.1 Materials

The WPP is collected from our office on NRC, Egypt. All materials and reagents were applied without further purification.

2.2 WPP Recycling

The WPP were beaten with a traditional Valley-type laboratory beater (Voith Inc., Appleton, WI, USA) at 3% consistency and 25°C for 3 min. After being immersed in 1% NaOH (wt/wt) for 18 h. Next, the remnants were washed with water. In order to uniformize humidity, the squeezed pulps were placed into polyethylene bags and chilled for 24 h. Chlorous acid was used to bleach the pulp that resulted.

2.3 Preparation of CNTs from MB

5 g of MB were added to a ferrous, nickel, and cobalt nitrate solution with vigorously stirring for one hour. Then, 10% of urea in 20 mL of H_2O was added. The mixture was put into a stainless steel reactor and cooked for three hours at 180°C in an electrical muffle. After washing, it was dried. The following process involves wetting $Al(OH)_3$ with 5% $Fe_2(NO)_3$•$9H_2O$ and $Ni(NO)_3$•$6H_2O$ and heating it for 2 h at 750°C in the muffle. The catalyst was used to grind the hydrochar at an 800°C temperature in a stainless steel reactor, with a catalyst-to-hydrochar mass ratio of 10:1 for one hour. The product was cooled, then cleaned with 5 M HNO_3 and H_2SO_4, and finally dried with hot water [17].

2.4 Preparation of Recycled WPP Blended with CNTs

At first, WPP was suspended and homogenized by a homogenizer with water to obtain a homogenous suspension is made for 20 min. Then, 0.03 g of gelatin and different weights of the prepared CNTs (0, 0.01 & 0.02 g) are sonicated separately with 10 mL of pure water for 5 min to prepare CNTs/Gel dispersion.

After that, 0.3 g of WPP is added to the previous CNTs/Gel dispersions separately and stirred for 20 min. To create a WPP/CNTs/Gel sheet, the final three solutions are placed into three teflon plates and allowed to dry at room temperature. The prepared sheets are denoted as R1 (i.e., contains zero CNTs), R2 (contains 0.01 g CNTs) and R3 (contains 0.02 g CNTs) [22]. The resulting WPP/CNTs/Gel sheets' thickness is between 0.1–0.4 mm.

2.5 Characterization

The structural composition was analyzed using Raman spectroscopy (532 nm excitation) and Fourier-transform infrared spectroscopy (KBr pellet method). The mean hydrogen bond strength (MHBS) and the empirical crystallinity (LO) were calculated as follows:

$$\text{MHBS} = \frac{A_{OH}}{A_{CH}} \tag{1}$$

$$\text{LO} = \frac{A_{1425}}{A_{900}} \tag{2}$$

where A_{1425} and A_{900}, A_{OH} and A_{CH} refer to the FTIR absorbance at 1425, 900 cm^{-1} for OH and CH bands [36].

X-ray powder diffraction (XRD) analysis was conducted using a Bruker D-8 Advance diffractometer (Germany) to investigate crystallinity. The XRD patterns were obtained using copper (Kα) radiation (1.5406 Å) at a voltage of 40 kV and a current of 40 mA. The *d*-spacing, crystallite size, dislocation density, and microstrain were calculated from the XRD data.

$$d - spacing\ (d,\ nm) = \frac{\lambda}{2\ sin\theta} \tag{3}$$

$$Crystal\ size\ (D,\ nm) = \frac{0.9\ \lambda}{\beta\ Cos\theta} \tag{4}$$

$$Dislocation\ density\ (\sigma,\ \ nm - 2) = \frac{1}{D^2} \tag{5}$$

$$Micro\ strain\ (E) = \frac{\beta}{4\ \tan\theta} \tag{6}$$

where θ = Bragg's angle in radians, λ = X-ray wavelength (0.1542 nm) and β & θ are full widths at half maxima and Bragg's angle of the XRD peak, respectively [37,38].

TGA examination was performed by using a Perkin Elmer thermogravimetric analyzer at 1000°C with a rate of 10°C/min under N_2 atmosphere. Kinetics of thermal decomposition was explored for both of the prepared R1, R2 and R3 samples via the Coats-Redfern technique:

$$Log\left[\frac{1-(1-\alpha)^{1-n}}{T^2\ (1-n)}\right] = log\frac{AR}{\beta E}\left[1-\frac{2RT}{E}\right] - \frac{E}{2.303\ RT} \qquad for\ \ n \neq 1 \tag{7}$$

$$Log\left[\frac{-log(1-\alpha)}{T^2}\right] = log\frac{AR}{\beta E}\left[1-\frac{2RT}{E}\right] - \frac{E}{2.303\ RT} \qquad for\ \ n = 1 \tag{8}$$

where n is the order of degradation reaction, α is the fractional conversion, β (K/min) is the heating rate, T (K) is the temperature, R (kJ/mol.K) is the gas constant, A (s^{-1}) is the frequency factor and E is the activation energy [8,16]. The other kinetic parameters, including enthalpy (ΔH), entropy (ΔS) and free energy change (ΔG) were estimated employing Eq. (9).

$$\Delta H^* = E^* - RT, \Delta G^* = \Delta H^* - T\Delta S^* \text{ and } \Delta S^* = 2.303\left(log\frac{Ah}{KT}\right)R \tag{9}$$

where (h) and (k) are Planck and Boltzman constants [26,39].

The samples' morphology was examined using scanning electron microscopy (SEM) and transmission electron microscopy (TEM). The mechanical properties were performed by using 'Universal Testing Machine' model 4201. Young's modulus (YM), tensile strength (TS) and elongation at break (EB) were estimated by visual examination of the film breakage from linearity of the plot.

2.6 Flamabbility Test

Flammability tests were conducted on R1, R2, and R3 using the limiting oxygen index (LOI) method, following ASTM D-2863. The LOI values were determined for specimens measuring 100 mm × 52 mm × 0.3 mm with flame heights ranging from 6 to 25 mm. Vertical flammability was assessed using ASTM D6413/D6413M-15 on samples measuring 200 mm × 50 mm.

2.7 Computational Procedures

The Gaussian 09 W program was used to perform DFT calculations with a hybrid functional B3LYP with the 6-31G(d) basis set exhausted the Berny technique.

The total energy (E_T), the energy of highest occupied MO E_{HOMO}, the energy of lowest unoccupied MO E_{LUMO}, energy gap (E_g), dipole moment (μ), absolute electronegativity's (χ), chemical potentials (Pi), absolute hardness (η), absolute softness (σ), global electrophilicity (ω), chemical softness (S), and additional electronic charge (ΔN_{max}) will be calculated by [40]:

$$E_{gap} = (E_{LUMO} - E_{HOMO}) \tag{10}$$

$$\chi = \frac{-\ (E_{HOMO} + \ E_{LUMO})}{2} \tag{11}$$

$$Pi = \chi \tag{12}$$

$$\eta = \frac{(E_{LUMO} + \ E_{HOMO})}{2} \tag{13}$$

$$\sigma = \frac{1}{\eta} \tag{14}$$

$$S = \frac{1}{2\eta} \tag{15}$$

$$\Delta N_{max} = \frac{-Pi}{\eta} \tag{16}$$

$$\omega = \frac{Pi^2}{2\eta} \tag{17}$$

3 Results and Discussion

Fig. 1 illustrates the reaction mechanism between cellulosic WPP, gelatin, and CNTs involves hydrogen bonding between the hydroxyl (OH) groups of cellulose and the carboxyl (COOH) or hydroxyl groups of CNTs. Additionally, the amino (NH_2) groups of gelatin can react with the carboxyl groups of CNTs to form amide bonds (O=C–NH).

3.1 Computational DFT Study

DFT calculation was employed to study the stability of the WPP, gelatin, CNTs and WPP/CNTs/Gel. From Fig. 2 and Table 1, the results show that:

(a) The E_T of WPP/CNTs/Gel (7.277 au) is lower than WPP (1201.300 au), gelatin (1668.400 au) and CNTs (4532.800 au) which means that the formation of the WPP/CNTs/Gel releases energy. This released energy makes it harder to break the bonds in the composite, requiring more energy to burn it. Consequently, the WPP/CNTs/Gel exhibits greater resistance to fire, translating to high fire retardancy.

(b) The Pi for CNTs and WPP/CNTs/Gel are negative (i.e., −0.0868 and −0.196 eV) compared the cellulose and gelatin (i.e., 0.105 and 0.068 eV) which indicates the stability of CNTs and WPP/CNTs/Gel.

(c) From the calculations of the E_g is lower in the case of WPP/CNTs/Gel (i.e., 0.078 eV) which in turn prove the strong chemical reaction between WPP, gelatin and CNTs. Consequently, the lowering of the HOMO-LUMO energy gap is essentially a consequence of the large stabilization of the LUMO due to the strong electron-accepting capability of the electron-acceptor group (Fig. 2) [41].

(d) As shown in Table 1, the Pi is negative for CNTs and WPP/CNTs/Gel (i.e., −0.0868 and −0.196 eV) and it means that CNTs and WPP/CNTs/Gel are stable [42].

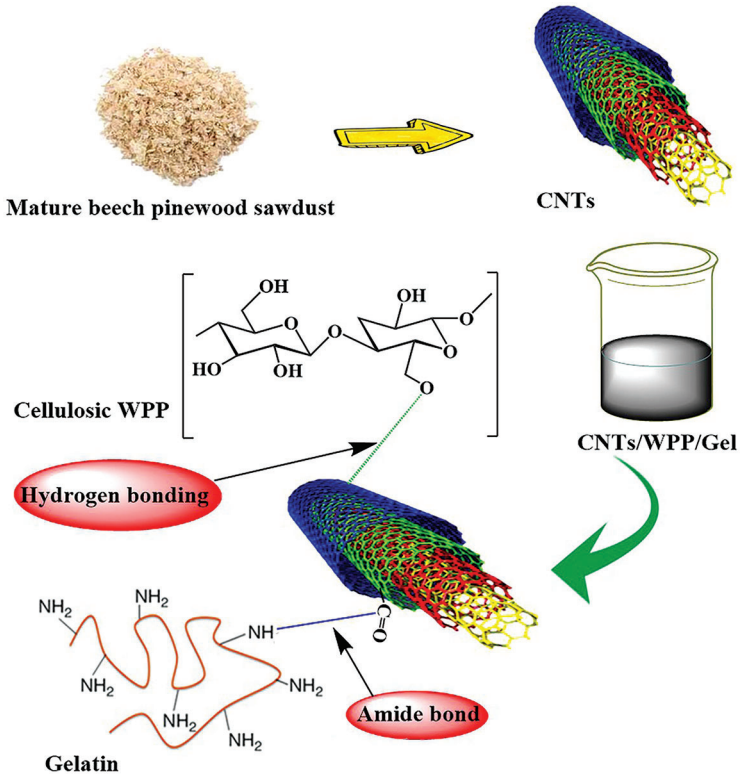

Figure 1: Reaction mechanism between WPP, gelatin and CNTs

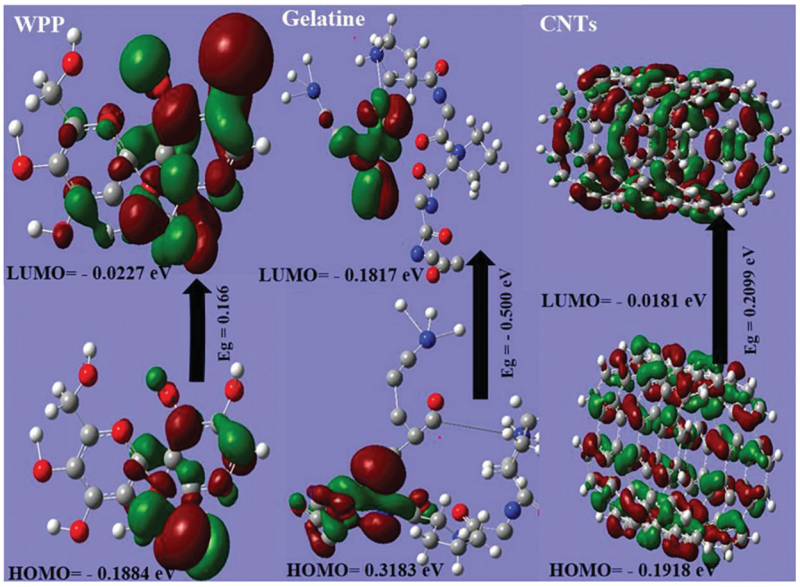

Figure 2: (Continued)

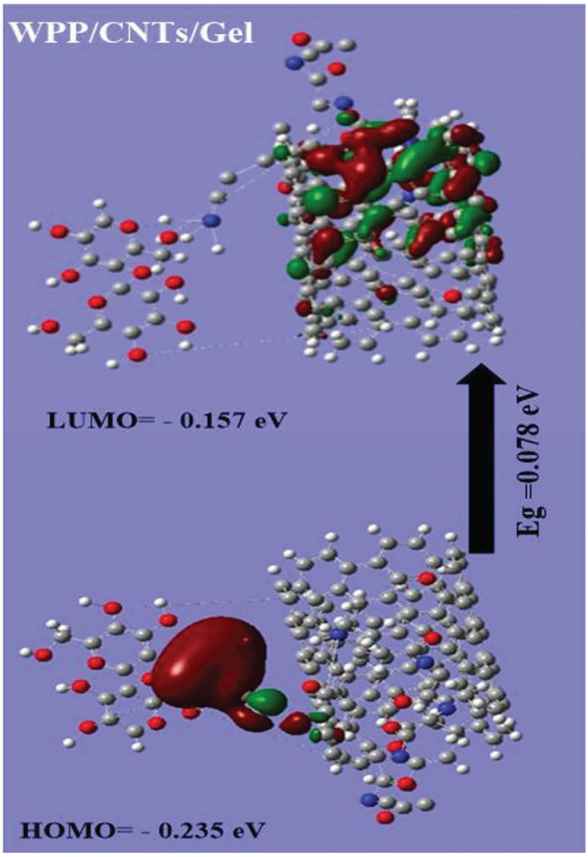

Figure 2: Gap energy (HOMO-LUMO) (eV) are calculated for hydrogel using DFT B3LYP/6-31G(d) and the molecular orbital's interaction between WPP, gelatin and CNTs

Table 1: The quantum chemical parameters of WPP, gelatin, CNTs and WPP/CNTs/Gel

DFT B3LYP/6-31G(d)	WPP	Gelatin	CNTs	WPP/CNTs/Gel
E_{LUMO} (eV)	−0.0227	−0.1817	−0.0181	−0.157
E_{HOMO} (eV)	−0.1884	0.3183	−0.1918	−0.235
E_T (au)	1201.300	1668.400	4532.800	7.277
E_g (eV)	0.166	−0.500	0.2099	0.078
μ (Debye)	15.710	44.820	0.0023	55.912
η (eV)	−0.083	−0.250	−0.1049	0.039
χ (eV)	0.083	−0.068	0.0868	0.196
Pi (eV)	0.105	0.068	−0.0868	−0.196
σ (eV)	−12.048	−4	−9.5283	25.641
ω (eV)	0.067	−0.009	0.0359	0.492
ΔN max	−1.273	−0.273	−0.8275	−5.025

All of the above reasons will influence on the flame retardancy in several ways. By making WPP/CNTs/Gel more difficult for molecules to participate in radical reactions and potentially promoting the formation of stable char layers, a lower HOMO-LUMO gap (i.e., E_g) can contribute to improved fire resistance.

3.2 Structural Characterization of the Prepared CNTs

3.2.1 Raman Spectra

The D-band is positioned at 1340.50 cm^{-1}, while the G-band is placed at 1583.00 cm^{-1}. A small I_D/I_G peak value (i.e., 0.94) suggests a high purity while a high I_G/I_D peak value (i.e., 1.06) shows a high degree of wall graphitization and the type of CNTs is multiwalled CNTs [8]_ENREF_15. The produced CNTs displayed a 2D band at 2890 cm^{-1}, and the I_{2D}/I_G ratio was 0.2, confirming the presence of multi-layer G sheets (Fig. 3a) [17,37].

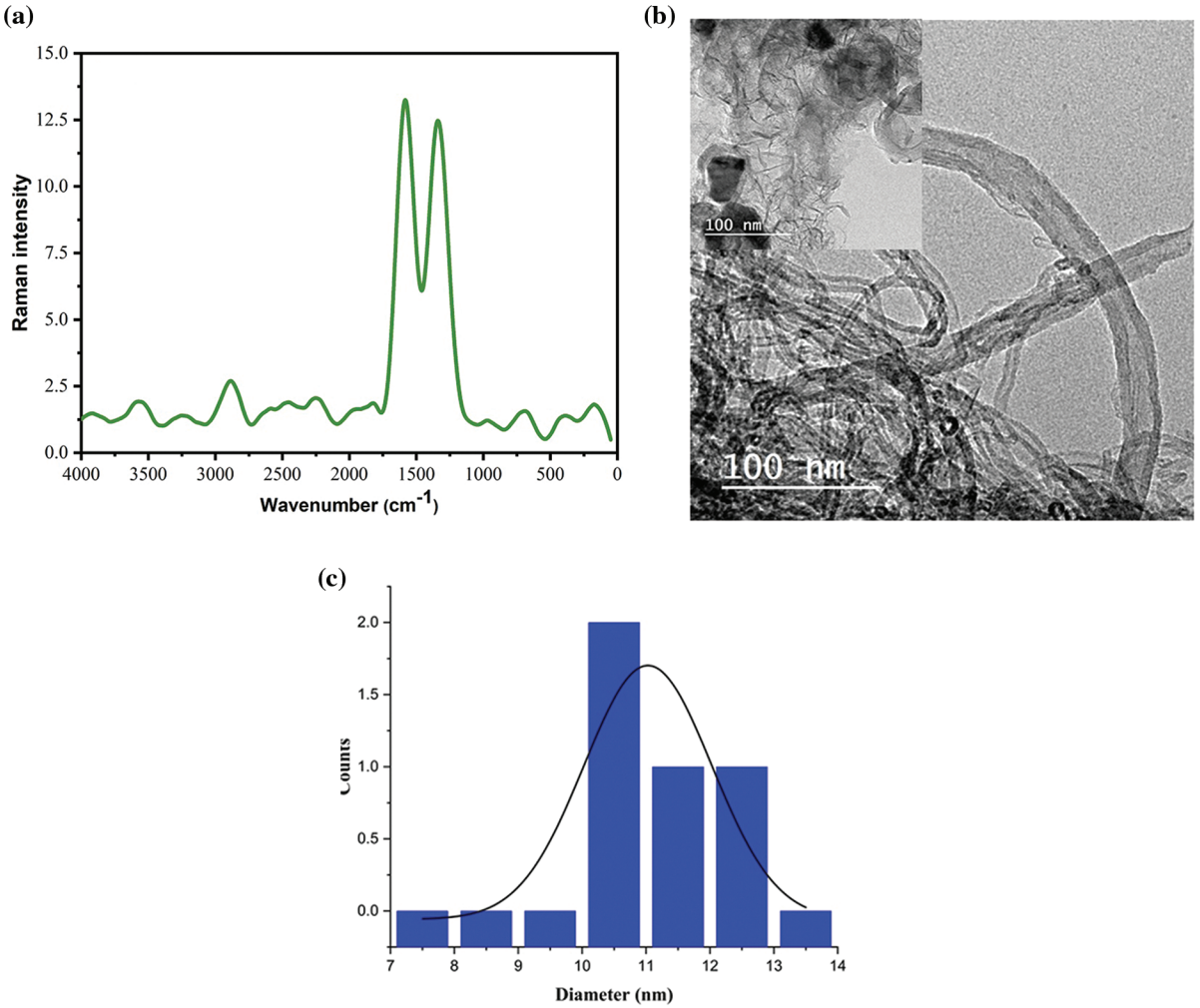

Figure 3: (a) Raman analysis, (b) TEM analysis. Inset: Another picture showing the presence of short CNTs with graphene sheets at the surface, and (c) particle size distribution of CNTs

3.2.2 TEM Analysis

TEM analysis for the prepared CNTs showed short bundles of CNTs bundles with diameter range ~7.5–13.5 and length range ~103.8–252.2 nm (Fig. 3b,c).

3.3 Structural Characterization of the Prepared Paper Sheets

3.3.1 FT-IR Analysis

Fig. 4 reveals FT-IR spectrum of CNTs' peaks which centered at 3437, 2932, 1634, 1427, 1217 and 1058 cm^{-1} which attributed to stretching vibration modes of OH, CH, C=O, O-C=O, C–O and C–O–C groups, respectively [17]. While, R1 shows peaks at 3299, 2925, 1631, 1548, 1448 and 1027 cm^{-1} which attributed to stretching of OH, CH, amide I of Gel (i.e., C=O & C–N), amide II of gelatin (N-H bending), C–O of cellulosic paper and C–O–C groups of cellulosic paper, respectively. R2 and R3 show peaks between 3278–3292, 2919–2921, 1627–1629, 1542–1546, 1434–1446 and 1025–1027 cm^{-1} related to stretching of OH, CH, C=O of CNTs & amide I of gelatin (i.e., C=O & C–N), O–C=O of CNTs and amide II of gelatin (N–H bending), C–O and C–O–C groups, respectively [25,43]. H-bonded OH stretching vibration of R1 appeared at 3288 cm^{-1} was shifted to lower frequency at 3284 and 3274 cm^{-1} for R2 and R3, respectively. Intermolecular H-bonding may be the cause of the shift in the absorbance value of the OH stretching vibration [44]. Decreasing C=O group intensity in R2 and R3 compared to CNTs confirmed the successful overlapping between amide of gelatin and carboxylate groups of CNTs [36]. The MHBS of CNTs, R1, R2 and R3 are summarized in Table 2. The C=O peaks for CNTs and R1 at 1634 and 1631 was shifted to lower wave numbers at 1629 and 1627 cm^{-1} for R2 and R3, respectively. This may be due to the interaction between C=O of CNTs with the amide or OH of WPP and Gel [45]. The ash (%) of R3 is the lowest one compared to others. This may be due to the high content of CNTs.

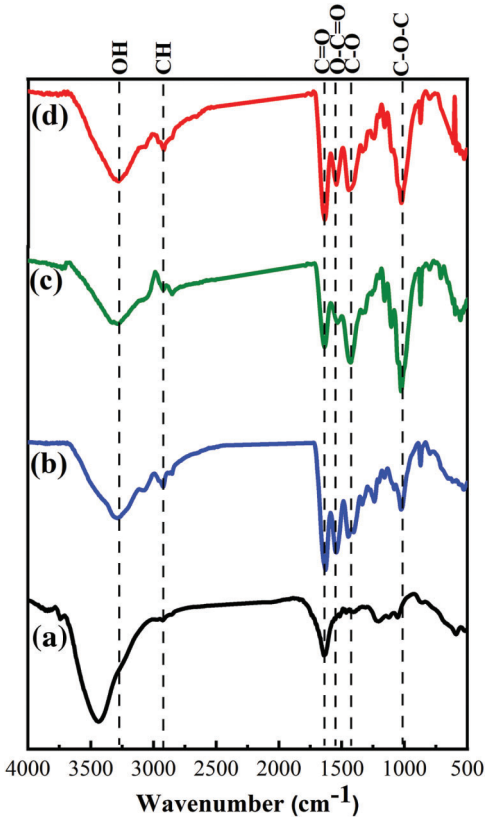

Figure 4: FTIR of (a) CNTs, (b) R1, (c) R2 and (d) R3

Table 2: Ash, LO and MHBS of CNTs, R1, R2 and R3

Sample	Ash (%)	LO (A_{1425}/A_{900})	MHBS (A_{OH}/A_{CH})
CNT	–	1.01	0.79
R1	94.47	0.95	0.94
R2	88.46	1.017	0.98
R3	63.66	1.003	0.98

3.3.2 X-Ray Diffraction

The prepared CNTs are composed of few CNTs and graphene (G) nano-sheets. The G nano-sheets have an amorphous peak at 2θ = 9.3 and 30.2° related to (001) and (002) diffraction peaks (Fig. 5a) [17]. The R1 exhibits four obvious diffraction peaks at 2θ = 11.55, 22.69, 29.40 and 35.83°, related to the (1–10), (110), (200), and (004) planes of cellulose. The triple helix of gelatin's triple peak is based on its inter-helix distance and the broad diffraction peak at 2θ = 22.69° is indicative of the amorphous portion of gelatin (Fig. 5b). When gelatin is attached to WPP, the diffraction peaks of gelatin might coincide with those of cellulose, but the diffraction patterns do not show any of the cellulose peaks [21].

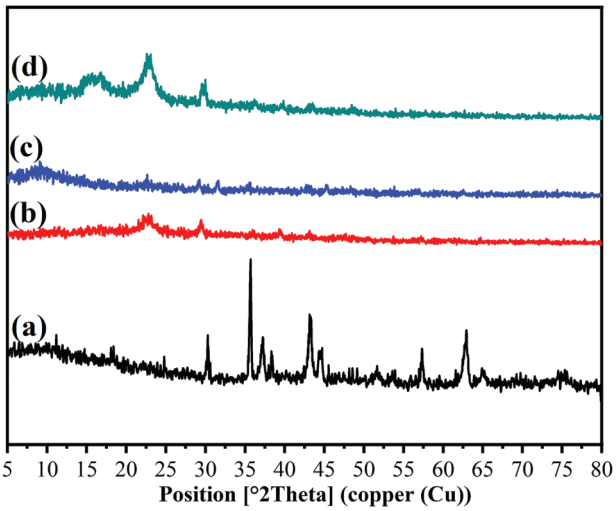

Figure 5: XRD analysis of (a) CNTs, (b) R1, (c) R2 and (d) R3

The d-spacing of R1 (3.91 nm) is increased compared to R2 and R3 (3.06 and 3.00 nm). The increased d-spacing in R1 was caused by the free, unmodified functional groups inserting themselves between the cellulose layers in the WPP. In contrast, the free functional groups in R2 and R3 were connected or linked to the incorporated CNTs [44]. While the D value reaches its peak in pure CNTs, it decreases as the CNT content in R3 increases. The variations in σ and ε exhibit contrasting trends. The combination of the lowest D value, highest σ, and highest ε in R3 (containing 0.02 g CNTs) can likely be attributed to the significant variability in d-spacing [46]. The Cr. I (%) for CNTs, R1, R2 and R3 were 14.63%, 14.83%, 18.75% and 31.32%, respectively (Table 3). The Cr. I (%) content of the modified sheets (R2 and R3) was notably higher than that of R1 (Fig. 5b–d). This increase can likely be attributed to the elevated concentration of CNTs, which influenced R1. The IR spectra and XRD Cr. I (%) values align with these findings.

Table 3: Crystallinity, d, D, σ and ε of CNTs, R1, R2 and R3

Sample	Cr. I (%)	Δ Cr. I (%)	d (nm)	D (nm)	σ (nm^{-2})	ε
CNTs	14.63	–	2.34	0.97	1.06	7.15
R1	14.83	–	3.91	0.088	129.13	2.25
R2	18.75	20.90	3.06	0.030	1111.11	45.66
R3	31.32	52.65	3.00	0.014	5102.04	110.30

3.3.3 SEM Analysis

Fig. 6 shows the surface morphology of CNTs, R1, R2 and R3, and how the modification process affected on R1 surface morphology. SEM analysis revealed that CNTs formed short, bundled structures. EDX analysis identified impurities including iron, cobalt, nickel, and molybdenum (Table 4). R1 exhibited a smooth surface without CNT coating, as depicted in Fig. 6b. In contrast, Fig. 6c,d shows CNTs covering the surfaces of R2 and R3 sheets, resulting in a rougher texture. The porosity of the films, calculated from SEM images and presented in Table 5, increased with higher CNT content. R2, with the highest CNTs concentration, displayed the highest porosity (69.10%) compared to R1 (68.80%) and R3 (70.44%). This increase in porosity can be attributed to the higher oxygen content associated with the increased CNTs.

3.3.4 Thermal Properties

TGA/DTG analysis at 1000°C showed that R1, R2, and R3 retained 48.58%, 38.90%, and 46.94% of their original mass, respectively, indicating the presence of non-volatile components. The R1's decomposition curve revealed two decomposition steps, whereas R2 and R3's decomposition curves revealed three steps. Thus, it can be concluded that the decomposition mechanisms of the untreated R1 and treated R2 & R3 sheets are different. The data from TGA/DTG, such as temperature at maximum rate of weight loss (T_{max}) and char yields at 300°C (C_{Y300}) and 700°C (C_{Y700}), are summarized in Table 6.

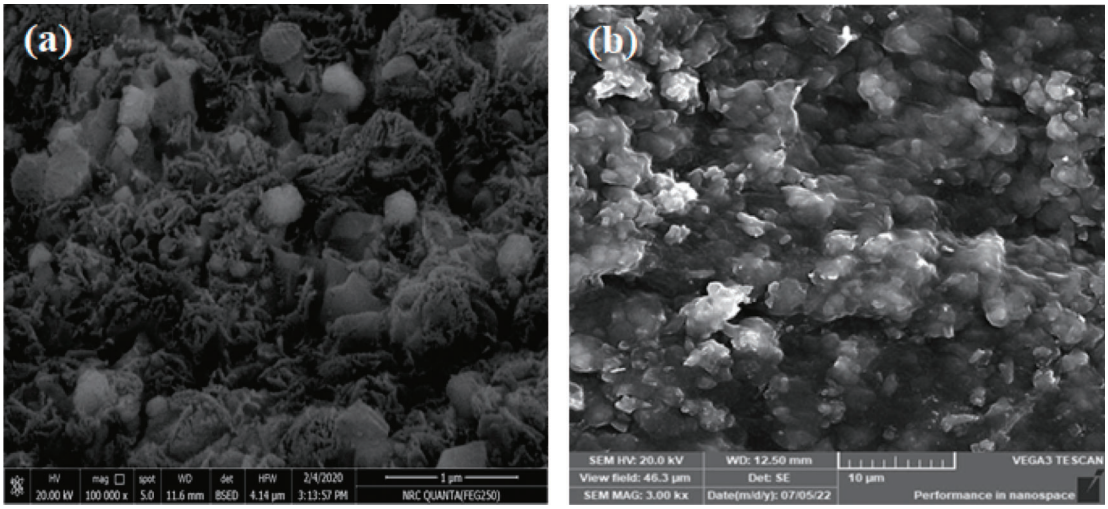

Figure 6: (Continued)

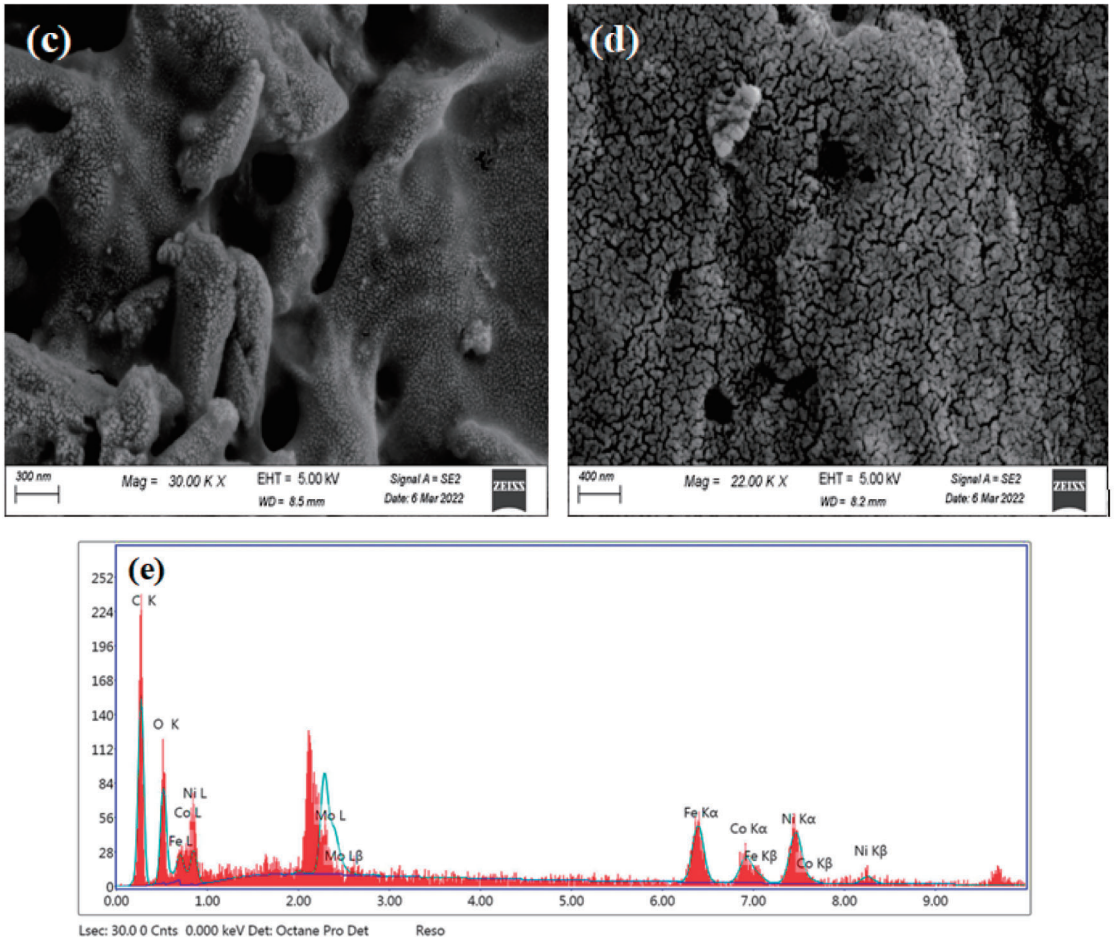

Figure 6: SEM analysis of (a) CNTs, (b) R1, (c) R2, (d) R3 and (e) EDX of CNTs

Table 4: Elemental composition of CNTs

Element	Weight (%)	Atomic (%)
C	43.46	66.43
O	20.04	23
Mo	8.2	1.57
Fe	9.47	3.11
Co	5.57	1.73
Ni	13.26	4.15

The thermal degradation processes of R1 could be separated into two key reaction phases. The 1st weight loss occurred between 41.84°C–212.41°C, with a maximum of 92.14°C, and mass loss (ML%) of 6.73% was probably brought on by the loss of moisture content [26,36]. The 2nd main decomposition step was between 210.86°C–984.31°C, with a maximum of 346.01°C, ∑**E** 12.15 kJ/mole and ML was

44.69%, ascribed to the depolymerizations and carbonization (Fig. 7a) [8,23]. The R2 and R3 have 1st decomposition steps at 41.94–150.04 and 41.88°C–205.83°C, with a maximum of 96.02°C and 97.63°C and ML was 4.51% and 7.95%, respectively, and ascribed to the moisture content. With an increase of the CNTs concentration, the initial thermal decomposition temperature of R2 and R3 increased compared to R1 due to the improved thermal stability by CNTs addition. The 2nd and 3rd main decomposition steps occur at temperatures of 185.36–465.63 & 207.66°C–483.35°C and 641.15–762.06 & 609.85°C–721.55°C, respectively [17,44].

Table 5: Porosity (%) of CNTS, R1, R2 and R3

Sample	Porosity (%)
CNTs	81.93
R1	68.80
R2	69.10
R3	70.44

Table 6: TGA/ DTG data of R1, R2 and R3

Sample	Stage	TGA range, °C	T_{max}, °C	Mass loss (%)	n	R^2	A (s^{-1})	ΔH (kJ mol^{-1})	Δ*s* (kJ mol^{-1})	Δ*G* (kJ mol^{-1})	C_{Y300}, (%)	C_{Y700}, (%)	E_a, (kJ mol^{-1})
R1	**1st**	41.84–212.41	92.14	6.73	1.5	0.836	0.22	32.18	–	129.52	13.54	53.50	35.31
	2nd	210.86–984.31	346.01	44.69	0.5	0.983	2.92	7.00	0.25–0.24	156.86			12.15
				∑ML %= 51.42						**ΔG = 286.38**			**∑E = 12.15**
				∑RW %= 48.58									
R2	**1st**	41.94–150.04	96.02	4.51	0.5	0.998	2.75	3.04	–0.23	88.18	13.97	56.35	6.01
	2nd	185.36–465.63	345.65	55.27	0.5	994	2.86	4.54	–0.24	154.42			9.68
	3rd	641.15–762.06	687.83	1.32	3.0	0.998	3.67	9.43	–0.24	243.73			17.41
				∑ML %= 61.10						**ΔG = 486.33**			**∑E = 27.09**
				∑RW %= 38.90									
R3	**1st**	41.88–205.83	97.63	7.95	1.5	0.981	0.36	8.71	–0.25	100.03	14.61	56.38	11.68
	2nd	207.66–483.35	346.92	43.98	1.5	0.968	0.30.	18.20	–0.26	179.99			23.35
	3rd	609.85–721.55	673.98	1.13	0.0	0.998	041	2.42	–0.26	250.38			10.29
				∑ML %= 53.06						**ΔG = 530.40**			**∑E = 33.64**
				∑RW %= 46.94									

Once the WPP was treated with CNTs, the C_{Y300} enriched by 103.17% and 107.90% for R2 and R3, respectively. Likewise, CY700 enriched by 105.32% and 105.38% for R2 and R3, respectively. From the results, treatment with CNTs decreased the amount of volatile products, formed during pyrolysis and diminished ML due to carbon combustion of R2 and R3 sheets compared to R1. Consequently, we speculated that the treatment with CNTs supports the production of carbonic char and retarded the degradation of cellulosic backbone of the recycled paper [17,38]. The main stage of R3 has a higher ∑E value (33.64 kJ mol^{-1}) compared to the ∑E values for the main stage of R1 (12.15 kJ mol^{-1}) and R2 (27.09 kJ mol^{-1}), which suggests that R2 and R3 has undergone thermal stabilization compared to

R1 [38,45]. This is a result of the blends' heterogeneity, which prevents heat energy from moving easily through the material. This demonstrates that the blends R2 and R3 have greater thermal stability than the neat R1 [46,47]. As a result, the heat reaction's course was affected by the CNTs present in the cellulose backbone in the recycled paper, which is what caused the E_a to vary. The information provided by MHBS and E_a agreed with each other. However, there was no consistency with the LO values; this may be because of the kind and strength of the created H–bonding [8]. This agree with DFT calculations from the calculations of the E_g is lower in the case of WPP/CNTs/Gel (i.e., 0.078 eV). A lowered E_g promotes the formation of a char layer. Char is a carbonaceous material that forms when organic matter decomposes under high temperatures. Char layers can act as a barrier to heat and oxygen, helping to prevent the spread of flames and reduce the rate of combustion. which in turn proves the strong chemical reaction between WPP, gelatin and CNTs.

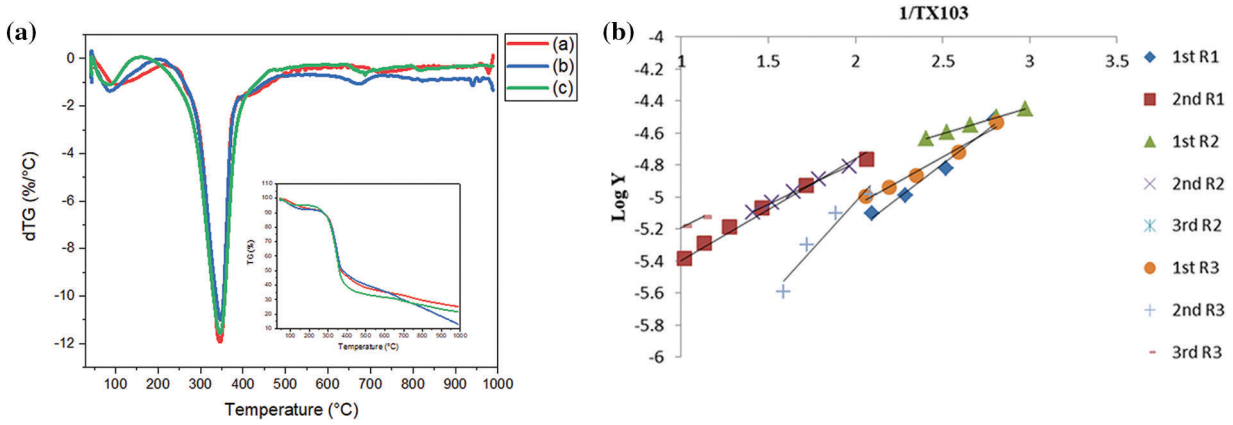

Figure 7: TGA/DTG of (a) R1, R2 and R3, (b) kinetics of thermal analysis

According to Table 6, the values for R1, R2, and R3's ΔS are negative, indicating that the system degradation won't happen naturally [17,36]. Additionally, as the reaction progresses, the value of ΔH for the R3 falls from between 8.71 and 18.20 kJ mol^{-1} at the beginning of the reaction to between 2.42 kJ mol^{-1} at the end, indicating a relatively low energy need (i.e., E_a was 11.68, 23.35 kJ mol^{-1} for the 1st and 2nd stages then decreased to 10.29 kJ mol^{-1} for the final stage). For R1, it was found that with lowering n (0.5) value, the ΔH was decreased (7.00 kJ mol^{-1}). This suggests that the pure R1 may decay with only a small amount of energy [17].

The noticeable drop in ΔH for the pure R1 can be attributed to the existence of free hydroxyl and carboxyl terminal groups, which are regarded as excellent leaving groups. The R1's bifunctionality (i.e., the existence of both COOH and OH groups), which has a high possibility of crosslinking, also leads to a drop in ΔH. for the gelatin-and CNT–containing WPP. The ΔG of R1, R2, and R3 are 286.38, 486.33, and 530.40 kJ mol^{-1}. The non-spontaneous reaction is indicated by the highest ΔG value, which is found in R3. The ΔG states that R3 requires more external heat input than R1 and R2 (Fig. 7b).

3.3.5 Mechanical Properties

The YM, EB, and TS are shown in Table 7 at maximum R1, R2, and R3 load. The results show that at 10% and 20% CNT loading, the addition of CNTs enhanced the maximal TS (by 16.93% and 283%) for R2 and R3. More pores produced at the surface and pore deficiencies throughout the thickness may be the cause of the significant rise in TS for R3 (it is also proved by SEM analysis). The substantial standard deviation values at 20% CNT loading (R3) can be attributed to the films' high porosity [17]. The addition of CNTs, however, clearly reduced the YM% of R1, R2, and R3, particularly at a 20% loading of CNT

(R3), where the reduction in YM% was 33% and 71% for R2 and R3, respectively (Fig. 8). As CNT loading was increased to higher levels, the YM values declined. This might be because larger CNTs concentrations result in enhanced stiffness properties. The decreasing YM of R3 provided evidence that CNTs were being used for nano-reinforcement [48,49].

Table 7: Mechanical properties of R1, R2 and R3

Sample	TS (MPa)	EB (%)	YM (MPa)
R1	1.24	6.53	1331.67
R2	1.45	11.30	884.93
R3	4.76	8.67	384.74

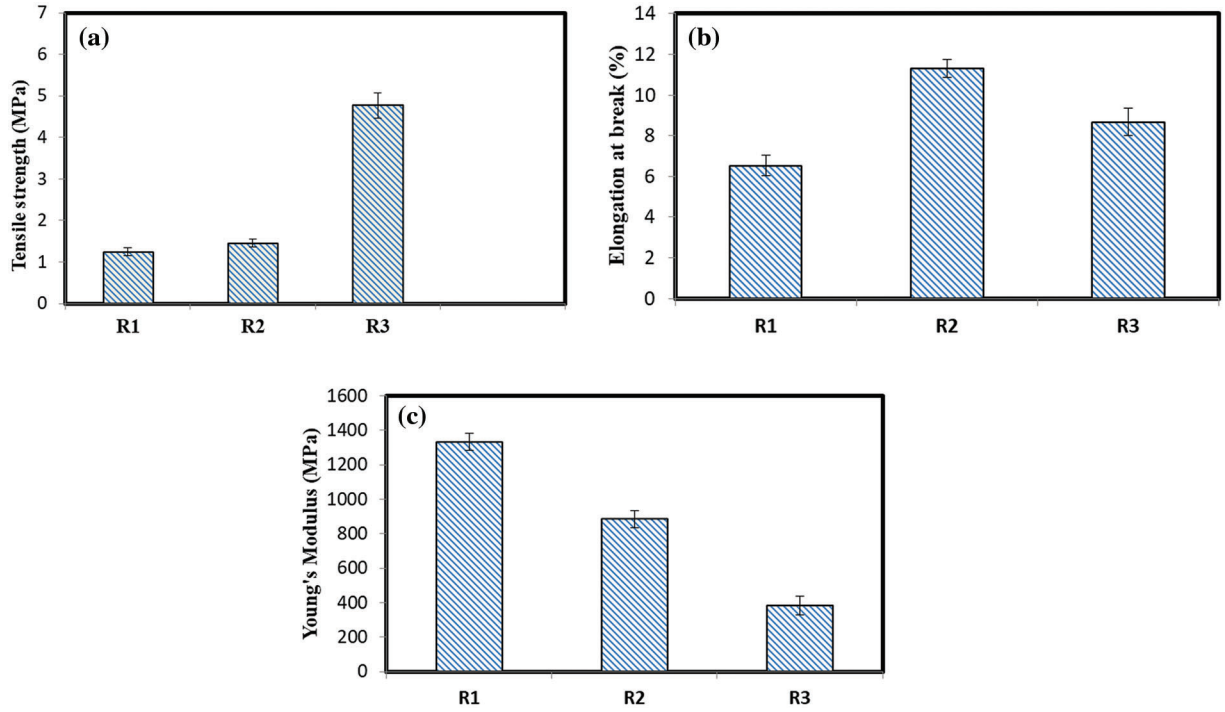

Figure 8: Mechanical properties of (a) R1, (b) R2 and (c) R3

As CNT loadings were increased to greater levels, the EB fell; for R3, it was roughly 33%, while it was still higher than that of the pristine R1. The EB of R2 increased up to 73%. The improvement in the films' mechanical properties suggests that the recycled paper matrix and CNTs surfaces are highly compatible. Data from TS, E_a, MHBS, and CrI% were all in agreement. This shows how the stiffness of the sheets formed is impacted by CNTs. When comparing the increase in TS and EB reached in the current work to the results previously reported, the advantage of using CNTs isolated from MB by direct hydrothermal treatment is obvious.

3.3.6 Flame Retardation

The flame retardancy test under continues exposure to the flame is performed on the R1, R2, and R3 sheets. An illustration of the burning process is shown in Fig. 9. All paper sheets of uniform thickness

are simultaneously ignited by a gas flame while resting on a metal support. The R1 sheet burns quickly, totally converting to ash in 6 s, whereas the R2 sheet takes 8 s to burn before changing to charcoal, demonstrating how the CNTs improve the sheet's flame retardancy (Fig. 9). On the other hand, the R3 sheet's burn time was extended up to 60 s. because it was the last to ignite. This is because R3 cannot thermally decompose in the presence of CNTs. It is predicted that the flame retardancy of the nanocomposites is significantly influenced by the CNTs network topologies on the WPP. The flame retardancy is appealing for use in industrial applications including packaging.

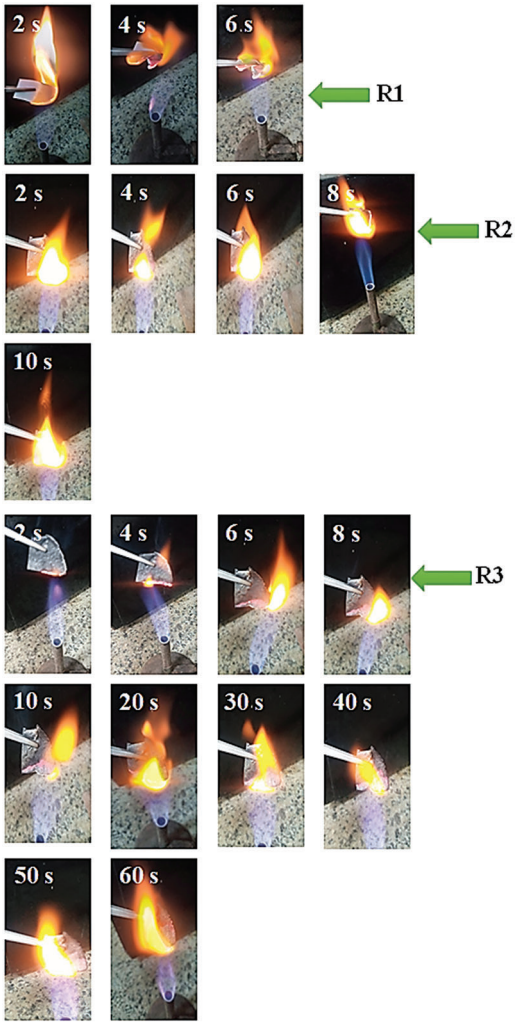

Figure 9: Photographs of flame retardancy test under continuous exposure to the flame for R1, R2 and R3

3.3.7 Flammability Testing

To assess the flame resistance of materials, the vertical burning test (UL94) and limited oxygen index (LOI) are widely used. The vertical burning test measures how easily a material ignites and how quickly flames spread. A rating of 0 indicates the highest level of flame resistance, while a rating of 5 suggests the lowest. Ratings between 1 and 5 mean that the material may not fully ignite, even if flames spread upward. The LOI determines the minimum oxygen concentration required for a material to burn in a mixture of oxygen and nitrogen.

The CNTs with varying concentrations, 0–0.02 gm (wt/wt) was used to enhance the thermal proofing properties of R2 and R3 sheets compared to R1. The vertical burning and LOI values of R1, R2 and R3 are presented in Table 8. When R3 exposed to flames, a protective carbon layer forms on the surface. This layer, strengthened by the presence of CNTs, acts as a shield, hindering the spread of flames and improving the material's fire resistance [32].

Table 8: Flame retardancy parameters of R1, R2 and R3

Sample	CNTs content (%)	LOI (vol. %)	Area of charred zone (cm^2)	Horizontal test	
				Rating (V)	Observation
R1	0	18.00	F	5	F
R2	3.33	19.20	40.00	3	F
R3	6.66	22.50	10.00	0	N–F

Note: F: Flammable; N–F: Non-Flammable.

From LOI results, we can observe that the LOI values for the treated recycled paper sheets increase with an increasing CNTs content from 0 to 0.02 gm (wt/wt). We can conclude that when the CNTs content increase, the flame retardancy increase. And since it is known that in order to achieve a level of flameproofing, the LOI value has to exceed 21 vol. % [21]. Accordingly, the larger LOI value for R3 corresponds to the better flame retardancy performance, whereas R1 and R2 sheets are combustible. The burning process of R1, R2 and R3 sheets at a 3 s ignition period in ambient air is shown in Fig. 10.

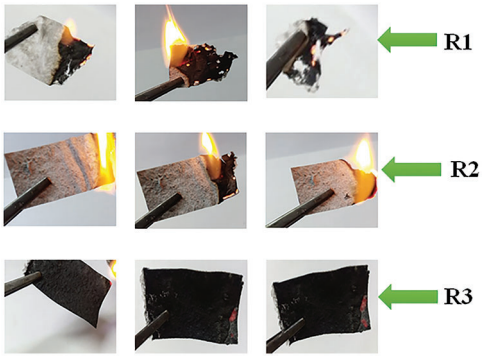

Figure 10: The burning process of R1, R2 and R3 with 3 s ignition period in ambient air

4 Conclusions

Recycling of waste should be encouraged as much as feasible because of the raw material shortage, energy crisis, and ecological pollution that the paper industry is currently facing. Due to these factors, cellulosic WPP was recycled into paper sheets with attractive qualities. This work offers a quick and efficient way to create CNTs/WPP/Gel sheets. At varied concentrations of CNTs which prepared from MB (0%, 15%, and 20%), the impact of CNTs on flame retardancy was examined. The findings demonstrate that crystallinity, porosity, mechanical strength, and flame retardancy are all improved, which makes CNTs an effective flame retardant for the recycled paper. The sheets have strengthened and become hard. At the optimal processing condition, better mechanical properties may be anticipated (i.e., R3). Because WPP, CNTs, and gelatin work well together; these sheets of CNTs and WPP demonstrate better thermal qualities (i.e., R2 and R3). The data obtained from TGA/DTG (T_{max}, C_Y, E_a) showed that treating WPP with CNTs makes them have higher thermal stability than the R1 sheets. This is consistent

with the information obtained from the flammability test. Our findings showed that as the concentration of CNTs increases the LOI values of R2 and R3 sheets increase. This means that the combustion in the R2 and R3 sheets with higher CNTs content which acted as a flame retardant turns to be not easy. Applications for the sheet will be expanded to bioscience and industrial uses because cellulose is biocompatible and biodegradable. Furthermore, the chemical interaction between WPP, gelatin and CNTs utilized in the DFT/B3LYP/6-31(G) basis set showed that the CNTs addition to the WPP and gelatin enhanced their stability and hydrogen bond interaction, which correlated with experimental analysis and investigated their HOMO–LUMO band energy gap.

From this we can conclude that the WPP sheets incorporating Gel and CNTs present a promising avenue for developing sustainable and cost-effective flame retardant materials. While the combination of these materials offers several advantages, including improved flame resistance and reduced environmental impact, further research and development are essential to address potential limitations such as consistency and long-term durability. By overcoming these challenges, these paper sheets could find widespread applications in various industries, particularly in packaging where their lightweight nature and customizable properties make them attractive options for enhancing fire safety. As sustainability and environmental concerns continue to grow, the development of innovative flame retardant materials like these will be crucial for meeting future demands.

Acknowledgement: The author appreciates the National Research Center for the financial support of this research activity.

Funding Statement: The research received funding from the PRIMA International Project, between the Academy of Scientific Research and Technology (ASRT) and PRIMA, through the Joint Agreement Project “Sustainable Antimicrobial Packaging Based on a Healthy Intelligent Renewable Approach” with acronym “SAPHIRA”.

Availability of Data and Materials: Not applicable.

Ethics Approval: None.

Conflicts of Interest: The author declares no conflicts of interest to report regarding the present study.

References

1. Koklukaya O, Carosio F, Grunlan JC, Wagberg L. Flame-retardant paper from wood fibers functionalized via layer-by-layer assembly. ACS Appl Mater Interfaces. 2015;7(42):23750–9. doi:10.1021/acsami.5b08105.
2. Yang HS, Kim DJ, Kim HJ. Combustion and mechanical properties of fire retardant treated waste paper board for interior finishing material. J Fire Sci. 2002;20(6):505–17. doi:10.1177/0734904102020006471.
3. Shatkin JA, Wegner TH, Bilek ET, Cowie J. Market projections of cellulose nanomaterial-enabled products–part 1: applications. Tappi J. 2014;13(5):9–16. doi:10.32964/tj13.5.9.
4. Siti S, Abdul HPS, Wan WO, Jawaid M. Bamboo based biocomposites material, design and applications. In: Materials science-advanced topics. IntechOpen; 2013. doi:10.5772/56057.
5. Bajpai P, Bajpai P. Options for utilization of waste. Manage Pulp Paper Mill Waste. 2015;3:79–180. doi:10.1007/978-3-319-11788-1_6.
6. Lam YL, Kan CW, Yuen CWM. Developments in functional finishing of cotton fibres-wrinkle-resistant, flame-retardant and antimicrobial treatments. Text Prog. 2012;44(3–4):175–249. doi:10.1080/00405167.2012.735517.
7. Pal A, Samanta AK, Bagchi A, Samanta P, Kar TR. A review on fire protective functional finishing of natural fibre based textiles: present perspective. Cellulose. 2020;360:370. doi:10.19080/ctftte.2019.05.555705.

8. Moshood TD, Nawanir G, Mahmud F, Mohamad F, Ahmad MH, AbdulGhani A. Sustainability of biodegradable plastics: new problem or solution to solve the global plastic pollution? Curr Res Green Sustainable Chem. 2022;5:100273. doi:10.1016/j.crgsc.2022.100273.
9. Mujtaba M, Fraceto LF, Fazeli M, Mukherjee S, Savassa SM, de Medeiros GA, et al. Lignocellulosic biomass from agricultural waste to the circular economy: a review with focus on biofuels, biocomposites and bioplastics. J Clean Prod. 2023;402:136815. doi:10.1016/j.jclepro.2023.136815.
10. Aracri E, Blanco CD, Tzanov T. An enzymatic approach to develop a lignin-based adhesive for wool floor coverings. Green Chem. 2014;16(5):2597–603.
11. Vahabi H, Laoutid F, Mehrpouya M, Saeb MR, Dubois P. Flame retardant polymer materials: an update and the future for 3D printing developments. Mater Sci Eng: R: Rep. 2021;144:100604. doi:10.1016/j.mser.2020.100604.
12. Iqbal M, Syed JH, Katsoyiannis A, Malik RN, Farooqi A, Butt A, et al. Legacy and emerging flame retardants (FRs) in the freshwater ecosystem: a review. Environ Res. 2017;152:26–42. doi:10.1016/j.envres.2016.09.024.
13. Cao Z, Chen Q, Li X, Zhang, Ren M, Sun L, et al. The non-negligible environmental risk of recycling halogenated flame retardants associated with plastic regeneration in China. Sci Total Environ. 2019;646:1090–6. doi:10.1016/j.scitotenv.2018.07.373.
14. Silva NG, Zanini NC, de Souza AG, Barbosa RF, Rosa DS, Mulinari DR. Halogen-based flame retardants in polyurethanes. In: Materials and chemistry of flame-retardant polyurethanes volume 1: a fundamental approach. USA: American Chemical Society; 2021. p. 141–71. doi:10.1021/bk-2021-1399.ch007.
15. Vojta Š., Bečanová J, Melymuk L, Komprdová K, Kohoutek J, Kukučka P, et al. Screening for halogenated flame retardants in European consumer products, building materials and wastes. Chemosphere. 2017;168:457–66. doi:10.1016/j.chemosphere.2016.11.032.
16. Hull T, Law R, Bergman Å. Environmental drivers for replacement of halogenated flame retardants. Polym Green Flame Retardants. 2014;46:119–79. doi:10.1016/B978-0-444-53808-6.00004-4.
17. Tohamy HAS, El-Sakhawy M, Elnasharty MM. Carboxymethyl cellulose membranes blended with carbon nanotubes/ag nanoparticles for eco-friendly safer lithium-ion batteries. Diam Relat Mater. 2023;138:110205. doi:10.1016/j.diamond.2023.110205.
18. Topçu E, Dağcı Kıranşan K. Flexible gold nanoparticles/rGO and thin film/rGO papers: novel electrocatalysts for hydrogen evolution reaction. J Chem Technol Biotechnol. 2019;94(12):3895–904. doi:10.1002/jctb.6187.
19. Qu Q, Xu J, Wang H, Yu Y, Dong Q, Zhang X, et al. Carbon nanotube-based intumescent flame retardants achieve high-efficiency flame retardancy and simultaneously avoid mechanical property loss. Polymers. 2023;15(6):1406. doi:10.3390/polym15061406.
20. Topçu E, Kıranşan KD. Electrochemical simultaneous sensing of melatonin and ascorbic acid at a novel flexible B-RGO composite paper electrode. Diam Relat Mater. 2020;105:107811. doi:10.1016/j.diamond.2020.107811.
21. Chai GQ, Zhu GQ, Gao Y, Zhou J, Gao S. Flame retardancy of carbon nanotubes reinforced carbon fiber/epoxy resin composites. Appl Sci. 2019;9(16):3275. doi:10.3390/app9163275.
22. Maria KH, Mieno T. Production and properties of carbon nanotube/cellulose composite paper. J Nanomat. 2017;2017:745029. doi:10.1155/2017/6745029.
23. Ngo T. Development of sustainable flame-retardant materials. Green Mater. 2020;8(3):101–22. doi:10.1680/jgrma.19.00060.
24. Mowafi S, Tohamy HAS. Application of electro-spun nano-fibers based on agriculture cellulosic biomaterial wastes for removal of dye and heavy metal from polluted water. J Textile Insti. 2024;2023:1–10. doi:10.1080/00405000.2023.2235495.
25. Abdel-Fatah AS, Tohamy HAS, Ahmed SI, Youssef MA, Mabrouk MR, Kamel S, et al. Anatase-cellulose acetate for reinforced desalination membrane with antibacterial properties. BMC Chem. 2023;17(1):112. doi:10.1186/s13065-023-01013-1.
26. Tohamy HAS. Fluorescence 'Turn-on' probe for chromium reduction, adsorption and detection based on cellulosic nitrogen-doped carbon quantum dots hydrogels. Gels. 2024;10(5):296. doi:10.3390/gels10050296.
27. Fujii M, Fujita T, Chen X, Ohnishi S, Yamaguchi N. Smart recycling of organic solid wastes in an environmentally sustainable society. Resourc Conservat Recycl. 2012;63:1–8. doi:10.1016/j.resconrec.2012.03.002.

28. Lee CK, Ibrahim D, Omar IC. Enzymatic deinking of various types of waste paper: efficiency and characteristics. Process Biochem. 2013;48(2):299–305. doi:10.1016/j.procbio.2012.12.015.
29. Belviso C, Montano P, Lettino A, Toschi F, Lambertini VG, Veca AD, et al. Determining the role of the method used to recycle polypropylene waste materials from automotive industry using sepiolite and zeolite fillers. J Mater Cycles Waste Manage. 2021;23:965–75. doi:10.1007/s10163-021-01184-w.
30. Sufian NAB. Mechanical properties of polypropylene mixed with rice husk polymer composites upon ultraviolet irradiation. Universiti Tun Hussein Onn: Malaysia; 2021. doi:10.46754/jssm.2021.10.005.
31. Xinsheng H, Yang G, Zhang Q. Application status and development prospects of bio-based flame retardants in packaging materials. Eur J Wood Wood Prod. 2023;81(6):1337–57. doi:10.1007/s00107-023-01977-w.
32. Trovato V, Sfameni S, Ben Debabis R, Rando G, Rosace G, Malucelli G, et al. How to address flame-retardant technology on cotton fabrics by using functional inorganic sol–gel precursors and nanofillers: flammability insights, research advances, and sustainability challenges. Inorganics. 2023;11(7):306. doi:10.3390/inorganics11070306.
33. Araby S, Philips B, Meng Q, Ma J, Laoui T, Wang CH. Recent advances in carbon-based nanomaterials for flame retardant polymers and composites. Compos Part B: Eng. 2021;212:108675. doi:10.1016/j.compositesb.2021.108675.
34. Xu L, Guo Z, Zhang Y, Fang Z. Flame-retardant-wrapped carbon nanotubes for simultaneously improving the flame retardancy and mechanical properties of polypropylene. J Mater Chem. 2008;18(42):5083–91. doi:10.1039/b808309f.
35. Wang X, Kalali EN, Wan JT, Wang DY. Carbon-family materials for flame retardant polymeric materials. Prog Polym Sci. 2017;69:22–46. doi:10.1016/j.progpolymsci.2017.02.001.
36. Tohamy HAS. Oil dispersing and adsorption by carboxymethyl cellulose-oxalate nanofibrils/nanocrystals and their kinetics. J Surfactants Deterg. 2024;27(1):147–60. doi:10.1002/jsde.12706.
37. Tohamy HAS, El-Sakhawy M, Hassan EB, Kamel S. Microwave-prepared quantum dots and their potential applications as adsorbents and chemosensors. Materials. 2023;16(20):6722. doi:10.3390/ma16206722.
38. Tohamy HAS, El-Sakhawy M, Kamel S. Fullerenes and tree-shaped/fingerprinted carbon quantum dots for chromium adsorption via microwave-assisted synthesis. RSC Adv. 2024;14(35):25785–92. doi:10.1039/D4RA04527K.
39. Viscusi G, Mottola S, Tohamy HAS, Gorrasi G, De Marco I. Design of cellulose acetate electrospun membranes loaded with N-doped carbon quantum dots for water remediation. In: IWA Regional Membrane Technology Conference, 2024; Palermo, Italy, Springer. doi:10.1007/978-3-031-63357-7_22.
40. Perveen M, Noreen L, Waqas M, Mehmood RF, Iqbal J, Manzoor S, et al. A DFT approach for finding therapeutic potential of graphyne as a nanocarrier in the doxorubicin drug delivery to treat cancer. J Mol Graph Model. 2023;124:108537. doi:10.1016/j.jmgm.2023.108537.
41. Akman F. Prediction of chemical reactivity of cellulose and chitosan based on density functional theory. Cellulose Chem Technol. 2017;51(3–4):253–62. doi:10.35812/cellulosechemtechnol.2019.53.24.
42. Rehman F, Khan AJ, Sama ZU, Alobaid HM, Gilani MA, Safi S. Surface engineered mesoporous silica carriers for the controlled delivery of anticancer drug 5-fluorouracil: computational approach for the drug-carrier interactions using density functional theory. Front Pharmacol. 2023;14:1146562. doi:10.3389/fphar.2023.1146562.
43. Abd El-Aziz M, Tohamy HAS, Youssef AM, El Desouky FG. Preparation and optimization of grafted hydroxyethyl cellulose, polypyrrole, and nitrogen-doped carbon quantum dots bionanocomposites for electrical, optical, and photoluminescence multicoloring applications. Int J Biol Macromol. 2024;278:134965. doi:10.1016/j.ijbiomac.2024.134965.
44. Tohamy HAS, El-Masry HM. Fluffy-like amphiphilic graphene oxide and its effects on improving the antibacterial activity and thermal outstanding of ethyl cellulose/polyvinyl alcohol hydrogel film. BMC Chem. 2024;18(1):116. doi:10.1186/s13065-024-01221-3.
45. Tohamy HAS, Mohamed FE-ZS, El-Sakhawy M. Novel microwave assisted carboxymethyl-graphene oxide and its hepatoprotective activity. BMC Pharmacol Toxicol. 2024;25:50. doi:10.1186/s40360-024-00768-0.

46. Kartick B, Srivastava SK, Mahanty S. TiS_2–MWCNT hybrid as high performance anode in lithium-ion battery. J Nanopart Res. 2013;15:1–12. doi:10.1007/s11051-013-1950-5.
47. Ramesan M. Thermogravimetric analysis, flammability and oil resistance properties in natural rubber and dichlorocarbene modified styrene butadiene rubber blends. React Funct Polym. 2004;59(3):267–74. doi:10.1016/j.reactfunctpolym.2004.02.005.
48. Campodoni E, Montanari M, Dozio SM, Heggset EB, Panseri S, Montesi M. Blending gelatin and cellulose nanofibrils: biocomposites with tunable degradability and mechanical behavior. Nanomater. 2020;10(6):1219.
49. Sennan P, Pumchusak J. Improvement of mechanical properties of poly(lactic acid) by elastomer. Malays J Anal Sci. 2014;18(3):669–75. doi:10.1016/j.desal.2013.06.012.